Characterizing the informativeness of pathogen genome sequence datasets about transmission between population groups

Cécile Tran-Kiem[1], Amanda C. Perofsky[2], Justin Lessler[3,4,‡], Trevor Bedford[1,5,‡]

1. Vaccine and Infectious Diseases Division, Fred Hutchinson Cancer Center, Seattle, WA, USA
2. Fogarty International Center, US National Institutes of Health, Bethesda, MD, USA
3. University of North Carolina at Chapel Hill, Chapel Hill, NC, USA
4. Johns Hopkins Bloomberg School of Public Health, Baltimore, MD, USA
5. Howard Hughes Medical Institute, Seattle, WA, USA

‡ denotes equal contribution.
Correspondence should be addressed to Cécile Tran-Kiem: ctrankie@fredhutch.org

Abstract

Pathogen genome analysis helps characterize transmission between population groups. The information carried by pathogen sequences comes from the accumulation of mutations within their genomes; thus, that the pace at which mutations accumulate should determine the granularity of transmission processes that pathogen sequences can characterize. Here, we investigate how the complex interplay between mutation, transmission, population mixing and sampling impacts the power of phylogeographic studies. First, we develop a conceptual probabilistic framework to quantify the ability of pairs of sequences in capturing migration history. This allows us to comprehensively explore the space of possible phylogeographic analyses by explicitly considering the pace at which mutations accumulate and the pace at which migration events occur. Using this framework, we identify a pathogen-intrinsic limit in the mixing scale at which their sequence data remains informative, with faster mutating pathogens enabling finer spatial characterization. Secondly, we perform a simulation study exploring a range of assumptions regarding sequencing intensity. We find that sample size further imposes a limit on the characterization of mixing processes. This work highlights inherent horizons of observability for population mixing processes that depend on the interaction between evolution, transmission, mixing and sampling. Such considerations are important for the design of phylogeographic studies.

Introduction

Pathogen sequencing is an invaluable tool for studying disease transmission patterns[1]. Analyzing pathogen genomes alongside metadata describing characteristics of infected hosts from which pathogens were isolated has helped characterize the transmission of pathogens between population groups of varying sizes. For example, hemagglutinin phylogenies have shed light on the inter-continental spread of seasonal influenza viruses[1], and patterns of occurrence of identical sequences have illuminated SARS-CoV-2 transmission between age groups[2].

It is generally acknowledged that the fundamental power of genomic epidemiological studies arises from the fast pace at which genetic variation is generated within pathogen genomes[3], relative to the pace at which pathogens transmit between hosts. When transmission and mutation events occur over similar timescales, pathogen genomes isolated from infected hosts indeed contain information about underlying epidemiological processes[4]. Thus, analysing such genomic data can help reconstruct transmission chains[5] or characterize population-level patterns of pathogen spread[1,2]. Prior work has explored the ability of pathogen genomes to reconstruct transmission chains[3,5], with overall resolution depending on evolutionary rate, generation time, transmission intensity and sampling effort. However, we still lack clear methods to evaluate both the power and limits of pathogen genome sequences in quantifying transmission at the population level (phylogeographic inference).

To study such population level processes, we expect the relative timescale at which mutation and migration events occur to be critical[6]. If mutations accumulate at a much slower pace than migration events occur (high migration / low mutation rate in Figure 1), genome sequences will be insufficient to infer migration patterns, as highlighted by the presence of large well-mixed polytomies in the phylogeny. Analyzing sequences from a faster mutating pathogen might enable characterization of such a migration process: although population mixing occurs rapidly, genome sequences will be sufficiently divergent to capture migration patterns (high migration / high mutation rate). Though insufficient to characterize rapid mixing processes, sequences from slow mutating pathogens still have the potential to decipher slow migration processes (low migration / low mutation rate).

Here, we develop a conceptual framework formalizing this intuition. Our model describes the ability of pathogen genome sequences to characterize pathogen spread between population groups. We apply this framework to a range of pathogens, characterized by distinct evolutionary characteristics and natural history parameters, and mixing processes (between age groups and various geographic scales). This approach enables us to identify fundamental limits in the ability of pathogen genome sequencing to capture transmission dynamics at the group level. Finally, we conduct a simulation study to characterize how factors such as sampling intensity impact phylogeographic signal across pathogens and mixing processes.

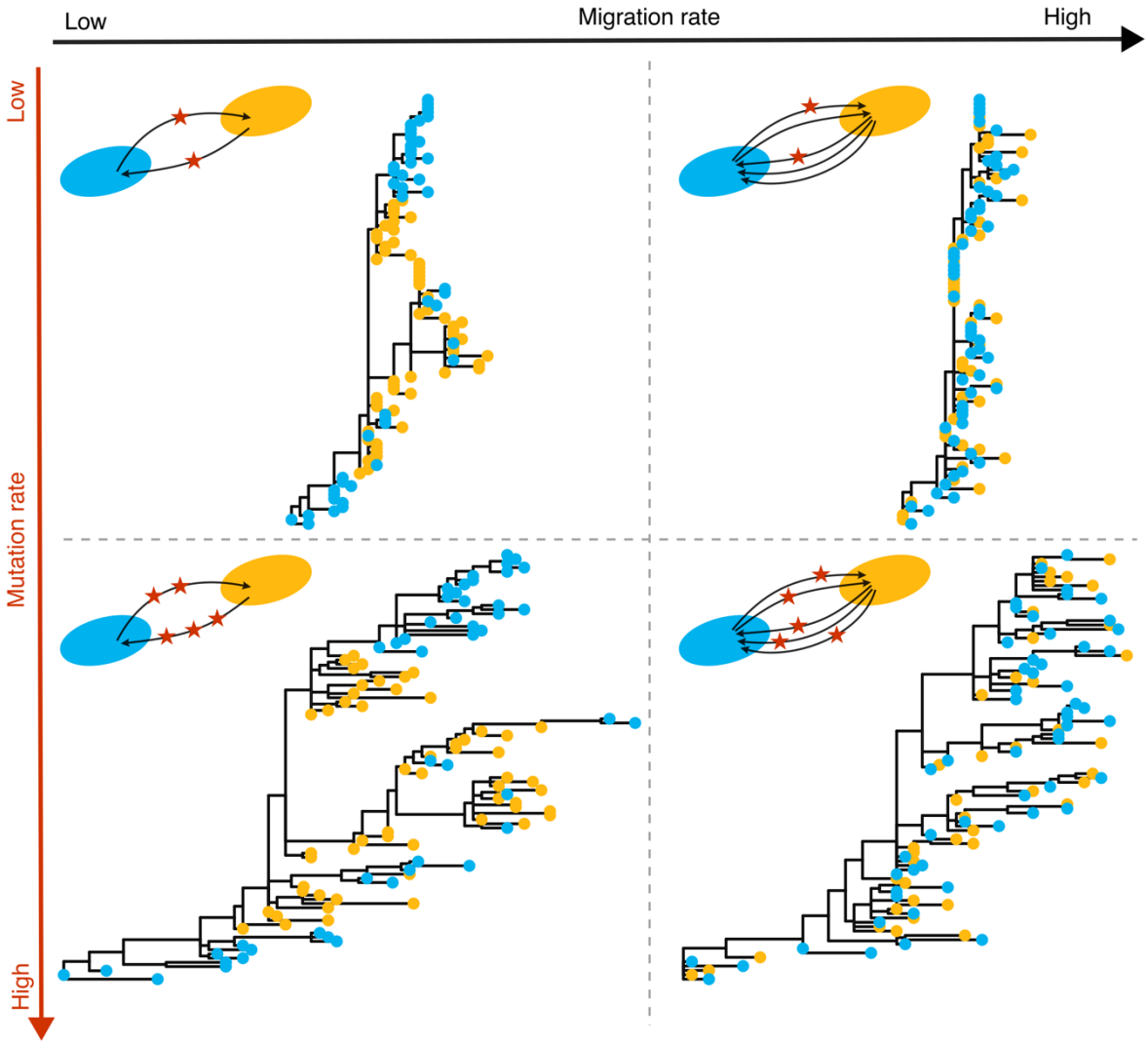

Figure 1: The ability of pathogen sequence data to characterize transmission between groups is impacted by the speed at which both migration and mutation events occur. To generate these illustrative figures, we simulate sequence data under an SEIR epidemic spreading between two population groups of size 1000 (yellow and blue). We assume a basic reproduction number of 1.5, that the mean time spent in the exposed compartment is 3 days, and that the mean time spent in the infectious compartment is also 3 days. 10% of infections are sequenced. We model the spread of a pathogen with a genome length of 3,000 bp. We simulate the evolutionary process for a low mutation rate scenario ($2 \cdot 10^{-5}$ mutations per bp per day) and a high mutation rate scenario ($8 \cdot 10^{-5}$ mutations per bp per day). For the migration process, we assume that infected individuals have a 98% probability of transmitting to someone within their group in the low migration scenario and a 50% probability in the high migration scenario. For each scenario, we include on the top left a toy figure to illustrate the frequency of migration events (number of arrows) and mutation events (number of stars).

Methods

Problem framing

We are interested in understanding the extent to which pathogen genome sequencing is informative about transmission processes at the group level. To do so, we define genomic *linkage criteria* between groups and evaluate how well they capture (true) transmission links. Specifically, we assume that two groups are genomically linked through an observed pair of sequences if the genetic distance between the elements of this pair of sequences lies below a defined genetic distance threshold Δ. We want to determine what is the sensitivity η_Δ, specificity χ_Δ and positive predicted value ϕ_Δ of this group linkage criterion.

Probabilistic framework

Notation. Let J denote the number of jumps between population groups (or migration events) separating two infected individuals. We assume that jumps occur under a Poisson process of rate λ, where λ is the migration rate. Let M denote the number of mutations between the infecting pathogens of these two infected individuals. We assume that mutation events occur under a Poisson process of rate μ, where μ is the per genome mutation rate. Let G be a random variable denoting the number of generations separating these two individuals. We assume that the generation time follows a Gamma distribution of shape α and scale β.

Distribution of the number of mutations conditional on the number of generations. Under these assumptions, we show that the number of mutations M conditional on the number of generations $G = g$ follows a negative binomial distribution of parameters[2]:

$$r_{M|g} = \alpha g$$

$$p_{M|g} = \frac{\beta}{\beta + \mu}$$

The full derivation is available in Supplementary Information.

Distribution of the number of jumps conditional on the number of generations. Similarly, the number of jumps J conditional on the number of generations $G = g$ follows a negative binomial distribution of parameters:

$$r_{J|g} = \alpha g$$

$$p_{J|g} = \frac{\beta}{\beta + \lambda}$$

The full derivation is available in Supplementary Information.

Distribution of the number of jumps conditional on the number of mutations. In practice, we don't observe the number of generations separating two infected individuals and are instead interested in the distribution of the number of jumps conditional on the number of mutations. Let $h(k; r, p)$ denote the probability mass function evaluated in k of a negative binomial distribution of parameters r and p. We introduce π_g the probability for two sequenced individuals of being g generations apart. By integrating over the possible number of generations separating two infections, we can show that:

$$P[J = j \mid M = m] = \frac{\sum_{g\geq 1} h(j;\ \alpha g,\ \frac{\beta}{\beta+\lambda}) \cdot h\left(m; \alpha g,\ \frac{\beta}{\beta+\mu}\right) \cdot \pi_g}{\sum_{g\geq 1} h\left(m; \alpha g,\ \frac{\beta}{\beta+\mu}\right) \cdot \pi_g}$$

The full derivation is available in Supplementary Information.

The distribution π_g of the number of generations between infected individuals is impacted by several factors, including the dynamics of the epidemic and the sampling scheme[7]. Wohl et al. used a simulation-based approach to approximate this probability distribution across a range of epidemiological scenarios, characterised by their reproduction number[7]. Their empirical estimates were obtained by simulating a branching process for $d = \ln(1000)\,/\ln\,(R)$ generations, (where R is the reproduction number). This corresponds to the number of generations required to reach an expected epidemic size of 1000. From this, they derive the empirical distribution of the number of generations separating two infections (which we denote $\hat{\pi}_g$). By design, the maximum number of generations separating two infected individuals in their simulations is therefore $g_{max} = 2d$ which depends on the reproduction number.

Here, we reuse the empirical probability distribution $\hat{\pi}_g$ they estimated to fully approximate the probability $P[J = j \mid M = m]$ as:

$$P[J = j \mid M = m] = \frac{\sum_{g=1}^{g_{max}} h(j;\ \alpha g,\ \frac{\beta}{\beta+\lambda}) \cdot h\left(m; \alpha g,\ \frac{\beta}{\beta+\mu}\right) \cdot \hat{\pi}_g}{\sum_{g=1}^{g_{max}} h\left(m; \alpha g,\ \frac{\beta}{\beta+\mu}\right) \cdot \hat{\pi}_g}$$

This also enables us to approximate the probability of two infected individuals being separated by j jumps and m mutations:

$$P[J = j] = \sum_{g=1}^{g_{max}} h\left(j; \alpha g, \frac{\beta}{\beta+\lambda}\right) \cdot \hat{\pi}_g$$

$$P[M = m] = \sum_{g=1}^{g_{max}} h\left(m; \alpha g, \frac{\beta}{\beta+\mu}\right) \cdot \hat{\pi}_g$$

Confusion matrix approach

Definition. To quantify the ability of a genetic linkage criterion to characterize transmission between population groups, we use a confusion matrix approach. We classify pairs of sequences depending on our ability to accurately capture migration history from their genetic sequences. Figure 2 illustrates how we define the true migration history between two sequenced individuals and the inferred migration history from sequence data. For example, on the top left, the sequences of our two sampled infections define a linked pair (the number of mutations separating their genomes is below a predefined threshold). The true migration history between these samples is *red* → *blue*. From our linked pairs, we infer that migration occurred between these two groups (*red* ↔ *blue*). The inferred migration history from sequence data therefore accurately captures the true underlying migration history, corresponding to a True Positive (TP). A False Positive (FP) corresponds to a situation where the inferred migration history doesn't match the actual migration one. Likewise, if a migration event to another group occurred between the sampled individuals defining the pair and the pair is not linked, that is a True Negative (TN), and if no other migration event occurred

between the two sampled individual and the pair is not linked, that is a False Negative (FN). Using our probabilistic framework, we can easily define the coefficients of the confusion matrix (Table 1).

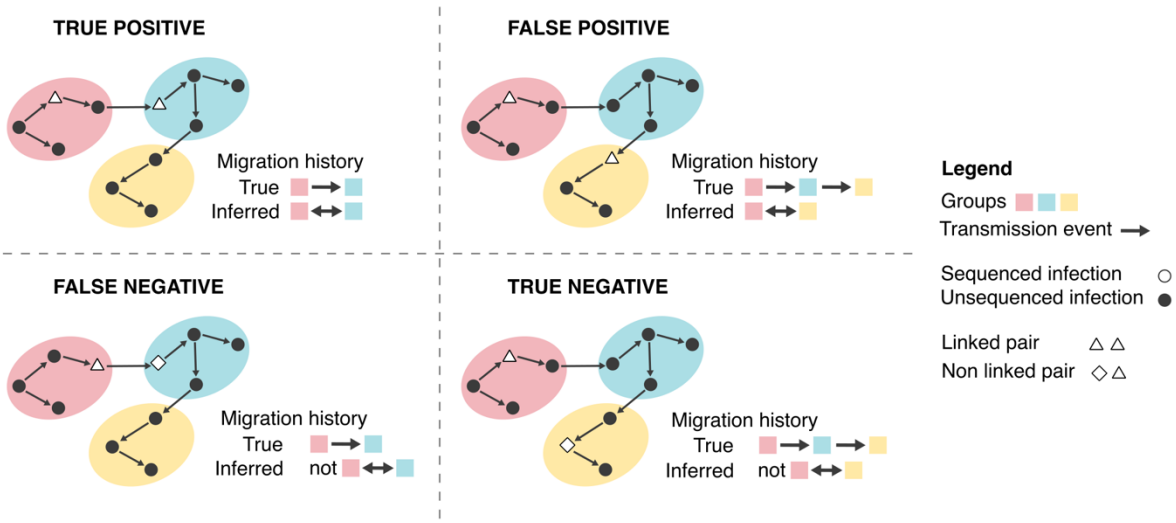

Figure 2: Illustration of the confusion matrix used to describe the ability of a genetic linkage criterion to capture the pathogen's migration history. These schematics illustrate a transmission chain propagating across three different groups of the population, each depicted by a colored oval shape. Each point (circle, triangle or diamond) corresponds to an infected individual, with white filled points indicating sequenced infections, and black filled points indicating infections that are not sequenced. The white filled points define a pair, that can be classified as True Positive, False Positive, False Negative or True Negative. For each diagram, we indicate the corresponding "true" migration history between the two sequenced individuals and the history inferred from the genomic linkage criterion.

Table 1: Coefficients of the confusion matrix for a linkage criterion based on a genetic distance threshold Δ.

	$J \leq 1$	$J > 1$
$M \leq \Delta$	True Positive (TP)	False Positive (FP)
$M > \Delta$	False Negative (FN)	True Negative (TN)

Sensitivity. The sensitivity η_Δ is the true positive rate. It measures how well our linkage criterion captures pairs of sequences that reflect the true migration history. From Table 1, we derive it as:

$$\eta_\Delta = P[M \leq \Delta \mid J \leq 1]$$

We show that we can compute it as:

$$\eta_\Delta = \sum_{d=0}^{\Delta} \eta_d{}'$$

where $\eta_d{}'$ is defined as:

$$\eta_d' = \frac{(P[J = 0 \mid M = d] + P[J = 1 \mid M = d]) \cdot P[M = d]}{P[J = 0] + P[J = 1]}$$

The full derivation is available in Supplementary Information.

Specificity. The specificity χ_Δ is the true negative rate. It measures the fraction of pairs not reflecting the true migration history that are not captured by the linkage criterion Δ. From Table 1, we can derive it as:

$$\chi_\Delta = P[M > \Delta \mid J > 1]$$

We show that we can compute it as:

$$\chi_\Delta = 1 - \sum_{d=0}^{\Delta} \chi_d{}'$$

where $\chi_d{}'$ is defined as:

$$\chi'_d = \frac{(1 - P[J = 0 \mid M = d] - P[J = 1 \mid M = d]) \cdot P[M = d]}{1 - P[J = 0] - P[J = 1]}$$

The full derivation is available in Supplementary information.

Positive predictive value. The positive predictive value (PPV) ϕ_Δ is defined as:

$$\phi_\Delta = P[J \leq 1 \mid M \leq \Delta] = \frac{P[M \leq \Delta \mid J \leq 1] \cdot P[J \leq 1]}{P[M \leq \Delta]} = \eta_\Delta \cdot \frac{P[J \leq 1]}{P[M \leq \Delta]}$$

It measures the proportion of linked pairs that correctly capture the migration history.

Characteristics of spatial and age-based transmission processes.

We apply our confusion matrix framework to a combination of pathogens and mixing processes to understand how analyzing the pathogen genome sequences of these different pathogens can provide insights on these population processes. We focus on transmission processes between geographies and age groups. To characterize these mixing processes, we use empirical data to estimate the probability that a jump (or migration event) occurs before a mutation one.

Age mixing from social contact data. We explore the probability for transmission to occur within the same age group using synthetic social contact data for Washington state from Mistry et al[8]. The latter study provides estimates of the mean daily number of contacts $M_{i,j}$ that individuals of age i have with individuals of age j (with one-year age bins). Let n_i denote the number of individuals of age i. Age groups can be defined by specifying an aggregation rule. This enables us to define the total number of contacts $\Gamma_{A,B}$ that occur within one day between two population groups A and B:

$$\Gamma_{A,B} = \sum_{i \in A} \sum_{j \in B} M_{i,j} \cdot n_i$$

We can also define $c_{A,B}$ the average daily number of contacts that individuals within age group *A* have with individuals in age group *B* as:

$$c_{A,B} = \frac{\Gamma_{A,B}}{\sum_{i \in A} n_i}$$

We compute the proportion $p^{within\ age}$ of contacts occurring within the same age groups across all contacts occurring within one day as:

$$p^{within\ age} = \frac{\sum_A \Gamma_{A,A}}{\frac{1}{2}\sum_A(\sum_{B \neq A} \Gamma_{A,B}) + \sum_A \Gamma_{A,A}}$$

The normalizing factor ½ is used to ensure each contact is only counted once. This metric is a summary statistic of assortativity at the population level for a specified level of age

aggregation. In practice, the probability for a contact of occurring within the same age group is not constant across age groups (Figure S1).

We compute values of $p^{within\ age}$ for different binning window size: 1-year, 2-year, 5-year, 10-year and 20-year age bins (Figure S2). For each binning scenario, aggregation starts from age 0 and stops at age 79. We systematically include an age group corresponding to individuals aged 80 and older.

Spatial mixing from mobility data. We estimate the probability for transmission of occurring within the same geographical region using mobile device location data from SafeGraph (https://safegraph.com/), a data company that aggregated anonymized location data from 40 million devices, or approximately 10% of the US population, to over 6 million physical places (points of interest, POIs). To do so, we estimate the probability for a movement of occurring within the same geographical unit, while exploring different scales in the US: states, counties, Public Use Microdata Areas (PUMAs), census tracts, and census block groups (CBGs).

At the state and county level, we use data processed in Pullano et al.[9] and made publicly available in the associated GitHub repository[10]. The authors report the proportion $p_{i,j}$ of movements of people leaving in county i that travel to county j, across different states and for a range of time windows. We focus here on data from January 2020. To estimate the proportion of movements that occur within the same county, we compute a population-weighted average of the proportion of movements occurring within the same county as follows:

$$p^{within\ county} = \frac{\sum_i p_{i,i} \cdot N_i}{\sum_i N_i}$$

where N_i is the population size of county i, derived from US Census data and made available in the R *covidcast* package[11]. Using a similar definition, we estimate the proportion $p^{within\ state}$ of movements that occur within the same state.

To compute this quantity for smaller geographical units (PUMAs, census tracts and CBGs), we rely on a Washington state (WA) focused dataset[12]. We use SafeGraph's Weekly Patterns dataset to estimate movements within and between WA geographies between January 2019 and June 2022. This dataset provides weekly counts of the total number of unique devices visiting a POI from a particular home location. We restrict our analysis to POIs that are consistently recorded in SafeGraph's panel throughout the study period.

To measure movement within and between CBGs, we extract the home CBG of devices visiting POIs and limited the dataset to devices with home locations in the CBG of a given POI (within-CBG movement) or with home locations in CBGs outside of a given POI's CBG (between-CBG movement). This methodology was also applied to census tracts and PUMAs to measure movement within and between these larger geographic units.

To adjust for variation in the size of SafeGraph device panel over time, we multiply raw weekly visits to POIs by a scaling factor, corresponding to the monthly ratio of each CBG, census tract or PUMA's respective county census population size to the number of devices in SafeGraph's panel with home locations within that county. We then compute the total number of visits between geographies by summing adjusted weekly counts across POIs, over the entire study period. We use these adjusted counts to compute the proportion of movements occurring

within the same county, PUMA, census tract andCBG in WA. Estimated values for the proportion of movements within each geographical unit are detailed in Table S1.

Relationship between the probability for the infectee to be in the same subgroup as the infector and the jump rate λ. Mixing between population subgroups is typically quantified from empirical data sources such as mobility data sources or social contact surveys. From these, we can derive the probability ω that a contact occurs within the same population subgroup. We can relate this probability to the jump rate λ using:

$$\omega = P[\,J = 0 \mid G = 1\,] = \left(\frac{\beta}{\beta + \lambda}\right)^{\alpha}$$

Therefore, for a known value of ω, the corresponding migration rate is equal to:

$$\lambda = \beta(\omega^{-\frac{1}{\alpha}} - 1)$$

We use ω values estimated from mobility and social contact data (detailed in the *Age mixing from social contact data* and *Spatial mixing from mobility data* sections above) to compare the ability of pathogen sequencing to characterize population mixing processes across pathogens.

Case study across a range of pathogens.

Evolutionary and transmission characteristics. We apply our confusion matrix approach to the following pathogens: Ebola virus, seasonal influenza virus A/H1N1pdm and A/H3N2, measles virus, MERS-CoV, mpox virus, mumps virus, RSV-A, SARS-CoV, SARS-CoV-2 (both pre and post-Omicron) and Zika virus. We assume that sequencing provides whole-genome sequences for all these pathogens. We use previously estimated values of the probability p that a transmission event occurs before a mutation one for these pathogens[13]. To include a slow-mutating pathogen in our analysis, we explore an additional scenario wherein only the hemagglutinin (HA) segment of the influenza A/H3N2 virus is analysed (corresponding to a 0.92 probability that a transmission event occurs before a mutation).

Epidemiological scenarios. In the derivations above, we showed that sensitivity, specificity and PPV depend on the distribution of the number of generations separating two individuals picked at random in the population. We use the empirical distributions generated by Wohl et al.[7] for reproduction numbers R of 1.3, 1.5 and 1.8, with results for R of 1.3 described in the main text and for R of 1.5 and 1.8 presented in Supplementary information (Figures S3 and S4).

Characterisation of the parameter space across pathogens.

To comprehensively explore trends across different pathogens and mixing processes, we apply our confusion matrix approach across a range of evolutionary and mixing parameters. We consider a pathogen with a generation time of mean 4.9 days and standard deviation 4.8 days. This corresponds to the values we used for SARS-CoV-2 (Omicron variant). Assuming a Gamma distributed generation time, this corresponds to a shape of 1.04 and scale of 0.21 days. This parametrization is arbitrary and simply provides a direct way to map evolutionary rates μ to values of the probability that transmission occurs before mutation p and mixing rates λ to values of within-group assortativity ω. We then compute sensitivity, specificity and PPV by varying p and ω between 0.01 and 0.99 with an increment of 0.01.

Simulation study to explore the relationship between power and sample size

To evaluate how sample size influences the ability to characterize transmission patterns between population groups from sequence data, we perform a simulation study using the ReMASTER BEAST package[14].

Parametrization of the simulations

We modelled SEIR epidemics characterized by a basic reproduction number of 2, with a rate out of the exposed (E) compartment of 0.33/day and a rate out of the infected (I) compartment of 0.33/day. This corresponds to a Gamma distributed generation time with shape $\alpha = 2$ and scale $\beta = 1/0.33$ day. We consider the spread of a pathogen characterized by a probability p that transmission occurs before mutation (exploring values ranging between 0.1 and 0.9 with an increment of 0.1) between 4 population groups each of size 50,000. This probability p and the parametrization of the generation time as a Gamma distribution enables us to define the per genome mutation rate as:

$$\mu^{per\ genome} = \beta(p^{-\frac{1}{\alpha}} - 1)$$

by using similar arguments to those in subsection *Relationship between the probability for the infectee to be in the same subgroup as the infector and the jump rate* λ. Assuming a Jukes-Cantor model of evolution, we derive the per site mutation rate (which is used in the simulations) as:

$$\mu^{per\ site} = \frac{1}{l} \cdot \mu^{per\ genome}$$

where l is the genome length. We run simulations assuming a genome length of 3,000 bp.

We consider group mixing processes characterized by assortativity parameters ω ranging between 0.1 and 0.9 with an increment of 0.1. We assume a symmetric mixing matrix between groups (detailed parametrization in Table S2).

We assume that a fraction p_{seq} of all infections are sequenced (exploring values of 0.001, 0.005, 0.01 and 0.05).

Relative risk metric performance

To assess the ability of sequences below a given genetic distance threshold to capture mixing patterns, we compute a relative risk (RR) metric which was introduced in prior work and that was shown to capture SARS-CoV-2 transmission patterns between age groups and geographies[2].

Let $H_{i,j}$ denote the Hamming distance separating two sequences indexed i and j, let S_i denote the population subgroup to which sequence i belongs. Let n denote the number of sequences in the dataset. We define the relative risk $RR_{A,B}^{\Delta}$ of observing two sequences less than Δ mutations away in population groups A and B as:

$$RR_{A,B}^{\Delta} = \frac{n_{A,B}^{\Delta} \cdot n_{\bullet,\bullet}^{\Delta}}{n_{A,\bullet}^{\Delta} \cdot n_{B,\bullet}^{\Delta}}$$

where (using $\mathbf{1}$ to denote the indicator function):

$$n_{A,B}^{\Delta} = \sum_{i=1}^{n}\sum_{j=1}^{n} \mathbf{1}_{\{H_{i,j}\leq\Delta\}} \cdot \mathbf{1}_{\{i\neq j\}} \cdot \mathbf{1}_{\{S_i=A\}} \cdot \mathbf{1}_{\{S_j=B\}}$$

$$n_{A,\bullet}^{\Delta} = \sum_{B} n_{A,B}^{\Delta}$$

$$n_{\bullet,\bullet}^{\Delta} = \sum_{A}\sum_{B} n_{A,B}^{\Delta}$$

In situations where there aren't any pairs of sequences observed in either subgroup A or subgroup B ($n_{A,\bullet}^{\Delta}$ or $n_{B,\bullet}^{\Delta}$ is equal to 0), $RR_{A,B}^{\Delta}$ is not defined. To be able to compute RRs even in situations of low pair counts, we rely on a modified RR, defined as:

$$\widetilde{RR}_{A,B}^{\Delta} = \frac{(n_{A,B}^{\Delta} + 1) \cdot (n_{\bullet,\bullet}^{\Delta} + 1)}{(n_{A,\bullet}^{\Delta} + 1) \cdot (n_{B,\bullet}^{\Delta} + 1)}$$

For each combination of p_{seq}, ω and p, we simulate 50 outbreaks with associated sequence data and compute modified relative risks ($\widetilde{RR}$) for thresholds Δ ranging between 0 and 15. We then compute the Spearman correlation coefficient between RRs and the daily migration probability between groups. In simulations where the standard deviation of the modified RRs is equal to 0, we set the correlation coefficient to 0 (RRs are not informative about migration probabilities). For each combination of p_{seq}, ω, p and Δ, we compute the median correlation across the 50 replicate simulations $\rho^{50}(p_{seq}, \omega, p, \Delta)$. To characterize the best inference performance for a given sequencing effort p_{seq}, we compute the maximum median correlation across Δ ranging between 0 and 15:

$$\rho^{50,max}(p_{seq}, \omega, p) = \max_{0\leq\Delta\leq 15} \rho^{50}(p_{seq}, \omega, p, \Delta)$$

We then characterize the minimum level of sequencing effort required to be able to reach a correlation threshold τ (50% and 90%) for each combination of ω and p as:

$$p_{seq}^{required\ \tau}(\omega, p) = \min_{p_{seq}\in\{0.001,0.005,0.01,0.05\}} \{p_{seq} \mid \rho^{50,max}(p_{seq}, \omega, p) \geq \tau\}$$

Results

Factors impacting the ability of a genetic linkage criterion of capturing transmission between population groups

We find that the performance of the linkage criterion between population groups varies across pathogens and is determined by the relative timescale at which mutation and transmission events occur (Figure 3A-C). For example, the sensitivity increases as the probability p that transmission occurs before mutation increases (corresponding to slower mutating pathogens, when scaling the mutation rate with the time it takes for each transmission generation to occur), while the specificity and the positive predictive value (PPV) decrease with p.

To further explore how other parameters impact linkage performance, we focus on a subset of the pathogens depicted in Figure 3A-C. We select this subset to ensure coverage of the full range of p: SARS-CoV (low p), SARS-CoV-2 (Omicron period – intermediate p) and Influenza A/H3N2 (HA only – high p). Figure 3D-F depict how varying the genetic distance threshold used to define the linkage criterion impacts overall performance across these three pathogens. We find that specificity and PPV are always maximised at low thresholds while sensitivity

increases as the threshold is relaxed. This is expected as a lower threshold will capture infections that are more epidemiologically linked and therefore less likely to misrepresent migration history. These lower thresholds however come at a sensitivity cost, as some relevant pairs will not be captured by a more conservative criterion.

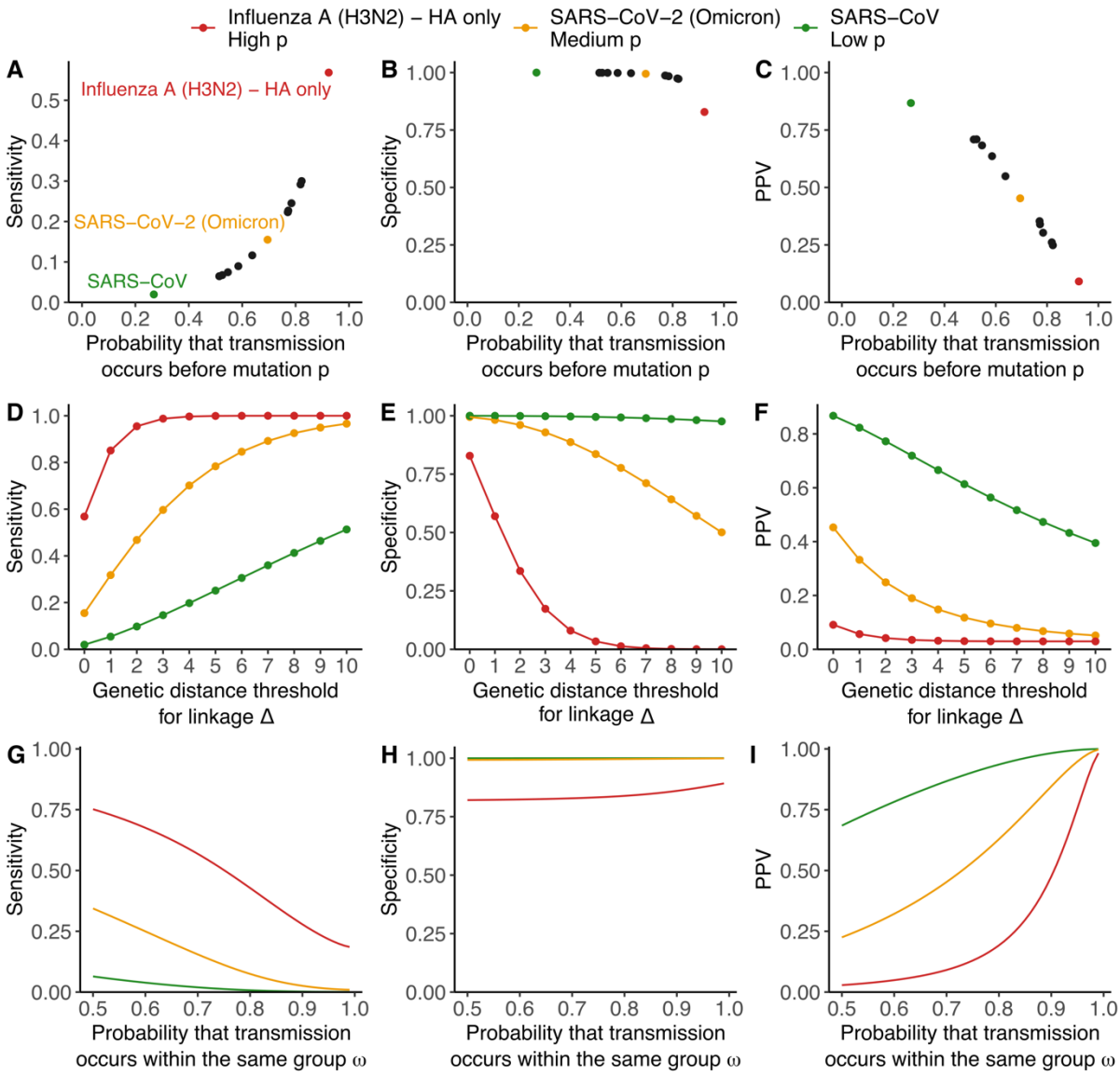

Figure 3: Impact of characteristics of the mutation and migration processes as well as the genetic distance threshold on the sensitivity, specificity and PPV. A. Sensitivity, **B.** specificity and **C.** PPV of a linkage criterion defined by $\Delta = 0$ assuming an assortativity parameter ω of 0.7 across pathogens and depicted as a function of the probability that a transmission event occurs before a mutation one across pathogens. **D.** Sensitivity, **E.** specificity and **F.** PPV as a function of the genetic distance threshold used to define the linkage criterion and assuming an assortativity parameter ω of 0.7. **G.** Sensitivity, **H.** specificity and **I.** PPV of a linkage criterion defined by $\Delta = 0$ as a function of the assortativity parameter ω.

As we are looking at the ability of a linkage criterion to characterize transmission between population groups, we expect the speed at which migration events (or mixing) occur to impact linkage performance. In Figure 3G-I, we explore the impact of the probability for an individual

to transmit within their group (measured by the assortativity parameter ω) on linkage performance. We find that faster mixing processes (characterized by lower assortativity values) are associated with higher sensitivities and lower specificities and PPVs than slower mixing processes, for a specified threshold Δ used to define linkage. This is expected because the probability for a pathogen to have moved several times between groups for a linked pair will increase as the assortativity parameter decreases (faster mixing processes), thereby leading to capturing pairs that are less representative of the migration history.

The computation of those coefficients is impacted by assumptions regarding the distribution of the number of generations separating two infected individuals in the population, and therefore the reproduction number. However, a sensitivity analysis varying the value of the reproduction number shows that overall trends are maintained (Figure S4).

Overall, these findings demonstrate that the ability for pathogen genome sequence data to characterize transmission between population groups depends on the interplay between evolutionary, transmission and migration processes.

Limits of genetic sequence data in their ability to characterize population processes

The PPV describes how often a pair of sequences separated by a Hamming distance less than Δ accurately captures migration history. For a given pathogen (characterized by its probability p that transmission occurs before mutation) and a transmission process of interest (characterized by its probability ω that transmission occurs within the same group), this PPV is highest for a genetic distance threshold Δ of 0 (Figure 3F). To explore the ability of consensus genome sequences in characterizing population processes, we computed the PPV for a threshold Δ of 0 as a function of both p and ω (Figure 4). To facilitate interpretability, we indicate on the left of the figure how different mixing processes map to the assortativity scale (ω) and on the top how different pathogens map to values of p.

The PPV for a genetic distance threshold Δ of 0 varies considerably across the phylogeographic parameter space. In our baseline epidemiological scenario, for a pathogen characterized by a p of 0.2, we estimate a PPV of 0.28 for a fast-mixing transmission process ($\omega = 0.2$) and a PPV of 0.93 for a slower mixing process ($\omega = 0.8$). By contrast, these PPVs drop to 0.02 ($\omega = 0.2$) and 0.44 ($\omega = 0.8$) for a pathogen characterized by a p of 0.8. We identify a region of low PPV in the phylogeographic parameter space, primarily in the region wherein values of p are higher than values of ω (lighter red colours in Figure 4). This corresponds to combinations of pathogens and mixing processes for which analysing consensus sequence data will not provide sufficient resolution to characterize the corresponding mixing process. Each pathogen is therefore associated with a horizon of observability regarding population mixing processes, that depends on the pace at which mutations accumulate within its genome.

Trade-off between sample size and positive predictive value

A high PPV ensures the signal from linked sequence pairs is as specific as possible and captures the true migration history. This PPV is maximized at low genetic distance thresholds Δ, but this comes at a cost of reducing the number of pairs used in the analysis, as lower

thresholds result in decreasing linkage probability (Figure 5). This underlines that the performance of our group linkage criterion cannot be considered in isolation from the composition and size of the dataset being studied. A low linkage probability and a high PPV may be preferred in a large dataset but may not be useful when analysing a smaller set of sequences, wherein only a few pairs of sequences ultimately meet the linkage criterion. The PPV therefore quantifies the informativeness of genome sequences about population mixing processes in situations where the sample size is large enough for low thresholds not to yield a critically low number of linked pairs.

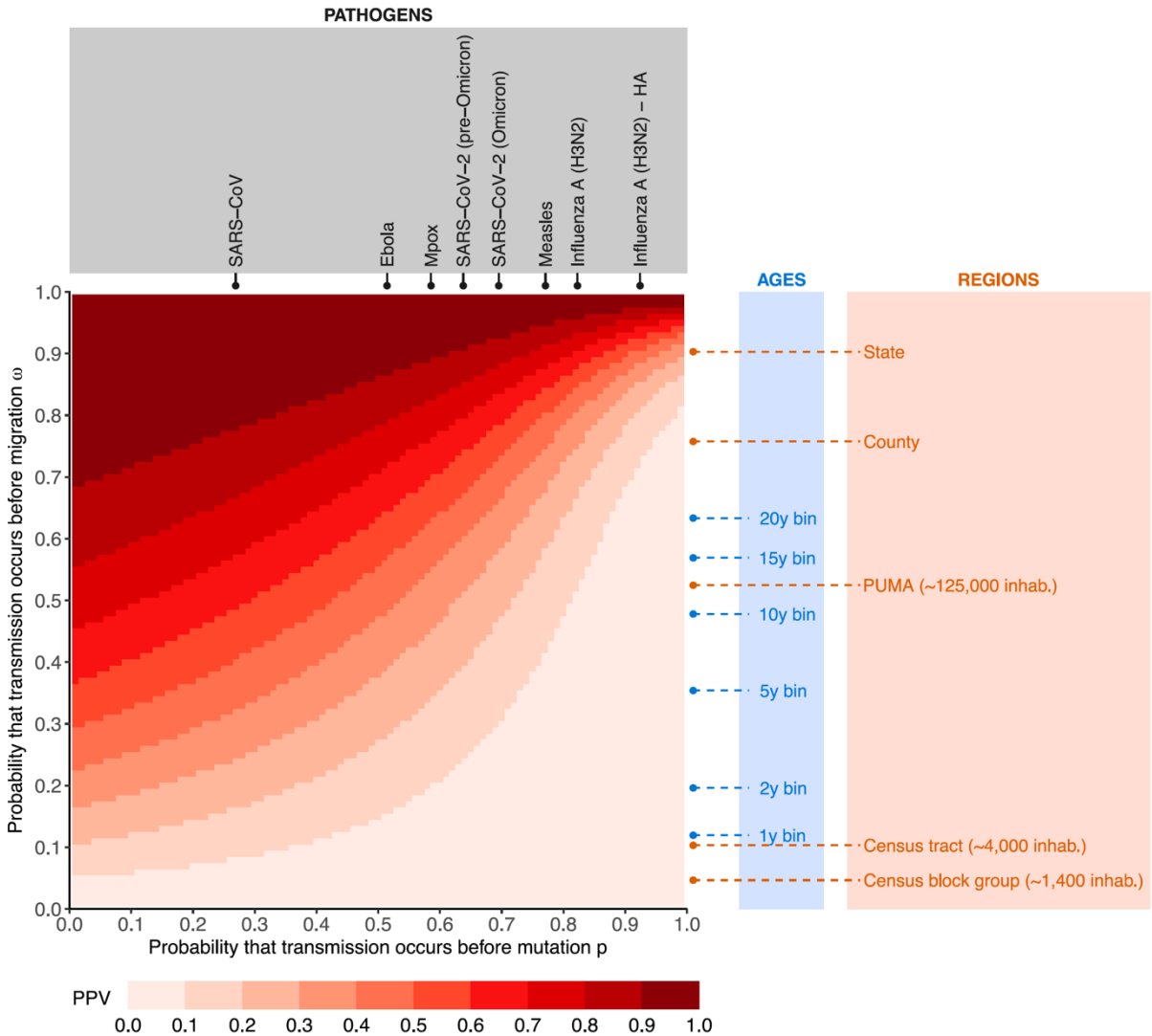

Figure 4: The relative timescale at which mutation and migration events occur determines the extent to which pathogen sequences are informative about migration processes. The heatmap depicts the positive predictive value associated with a threshold Δ of 0 as a function of the probability that a transmission event occurs before a mutation one p and the probability that a transmission event occurs before a migration one ω (assortativity parameters). For context, we indicate on the top values for p across a range of pathogens and on the right values for ω across a range of mixing process. Values are computed considering a pathogen with a generation time of mean 4.9 days and standard deviation 4.8 days and a reproduction number of 1.3 (baseline epidemiological scenario).

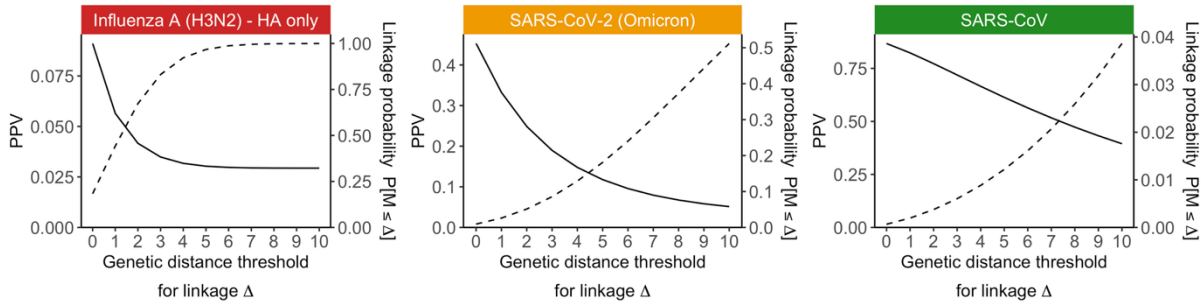

Figure 5: Sample size impacts the genetic distance threshold Δ that maximizes phylogeographic power. Impact of the genetic distance threshold Δ on the PPV (solid line) and the linkage probability $P[M \leq \Delta]$ (dashed line) assuming an assortativity parameter ω of 0.7 across pathogens.

To investigate how sample size impacts our ability to characterize mixing processes from pathogen sequence data, we simulate synthetic outbreaks and vary the sampling and sequencing of a fraction of all infected individuals. We then compute the correlation between the RR of observing pairs of sequences separated by less than Δ mutations and the migration probability between these population subgroups[2]. This RR metric quantifies the extent to which pairs of sequences lying below a distance threshold Δ are enriched in sequences coming from subgroups of interest. Prior work demonstrates that this metric could serve as an alternative to traditional tree-based phylogeographic methods[2] and the median correlation reported in Figure 6 corresponds to a measure of method accuracy.

We find that sample size is another important factor influencing the power of phylogeographic studies, with low sequencing fractions being associated with a lower accuracy (Figure 6). Despite the PPV being highest for a genetic distance threshold $\Delta = 0$, we find that relying on this threshold is not sufficient to characterize mixing processes at low sequencing rates (top left facets in Figure 6). Considering less restrictive distance thresholds can increase phylogeographic power (bottom left facets in Figure 6), by increasing the number of sequence pairs analysed (Figure S5). However, the number of sequences available and analysed imposes an upper bound on inference accuracy, regardless of the distance thresholds (Figure 7A). Figure 4 highlights a fundamental limit for phylogeographic inference, determined by the relative pace at which mutation and migration events occurred. Here, we show that study design imposes an additional constraint. While it is theoretically possible to characterize a transmission process characterized by an assortativity value $\omega \sim 0.5$ from a pathogen characterized by $p \sim 0.7$ (which is similar to assessing transmission between age groups defined in decade increments from SARS-CoV-2 sequences) (Figure 4), our simulations highlight that this requires a sufficiently high level of sequencing. For example, in our four-group transmission simulations, we find that sequencing 1% of the infected population would not yield an inference accuracy greater than 90%, and one would need to rely on at least 5% of infections being sequenced to be able to draw such inferences (Figure 7B).

Overall, this shows that the ability of pathogen genome datasets to decipher transmission between population groups is influenced by the complex interplay between sampling intensity and the relative timescale at which mutation and migration events occur.

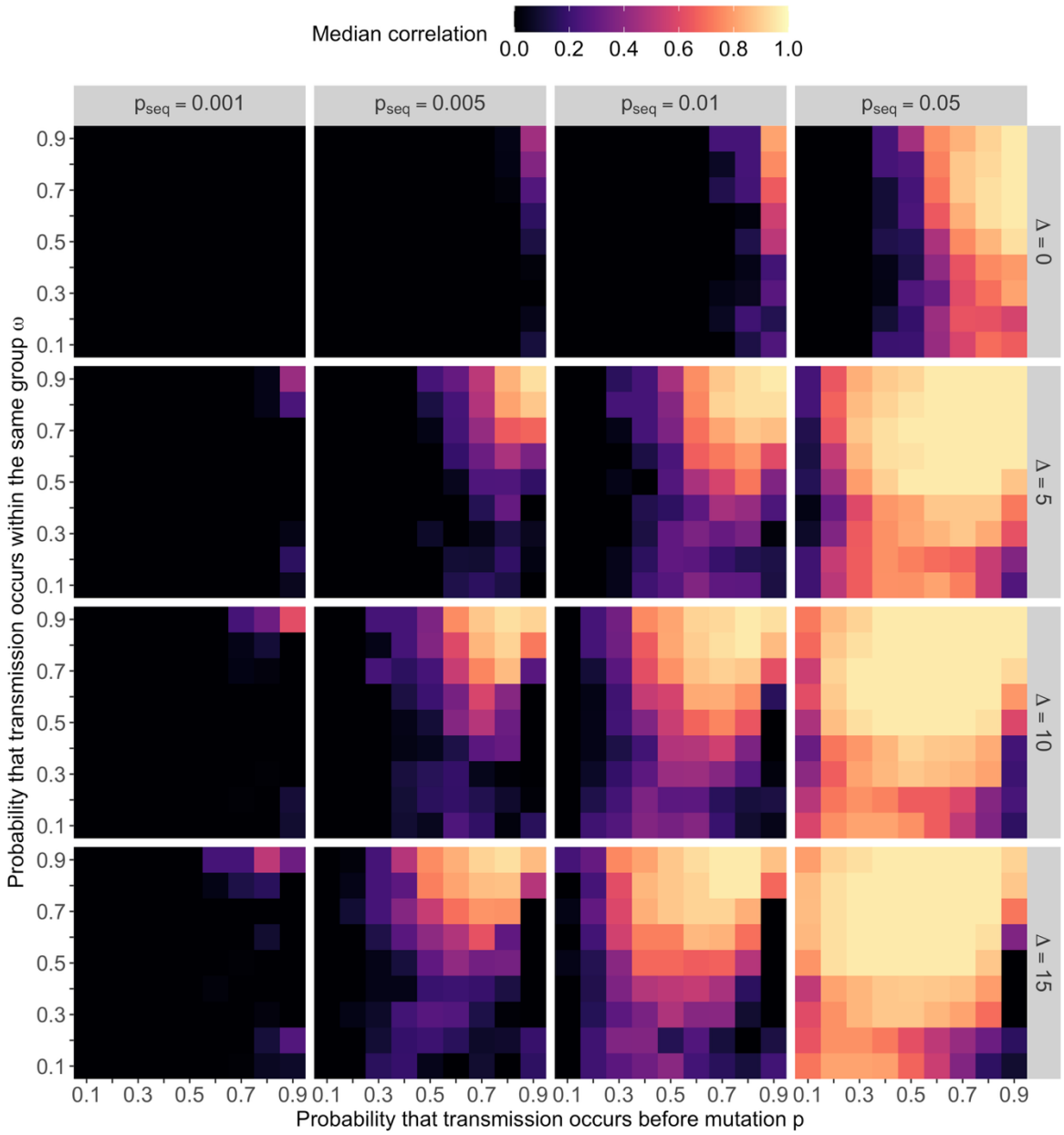

Figure 6: Impact of sample size and genetic distance threshold on phylogeographic inference accuracy. Median Spearman correlation coefficient (across 50 replicate simulations) between the RR of observing sequences less than Δ mutations away (rows) and migration probabilities between groups, across different sequencing fractions p_{seq} (columns). Results are displayed as a function of the probability p that transmission occurs before mutation and assortativity ω. When the median correlation is lower than 0, we display it as black (corresponding to 0) to improve visualization of positive median correlation values.

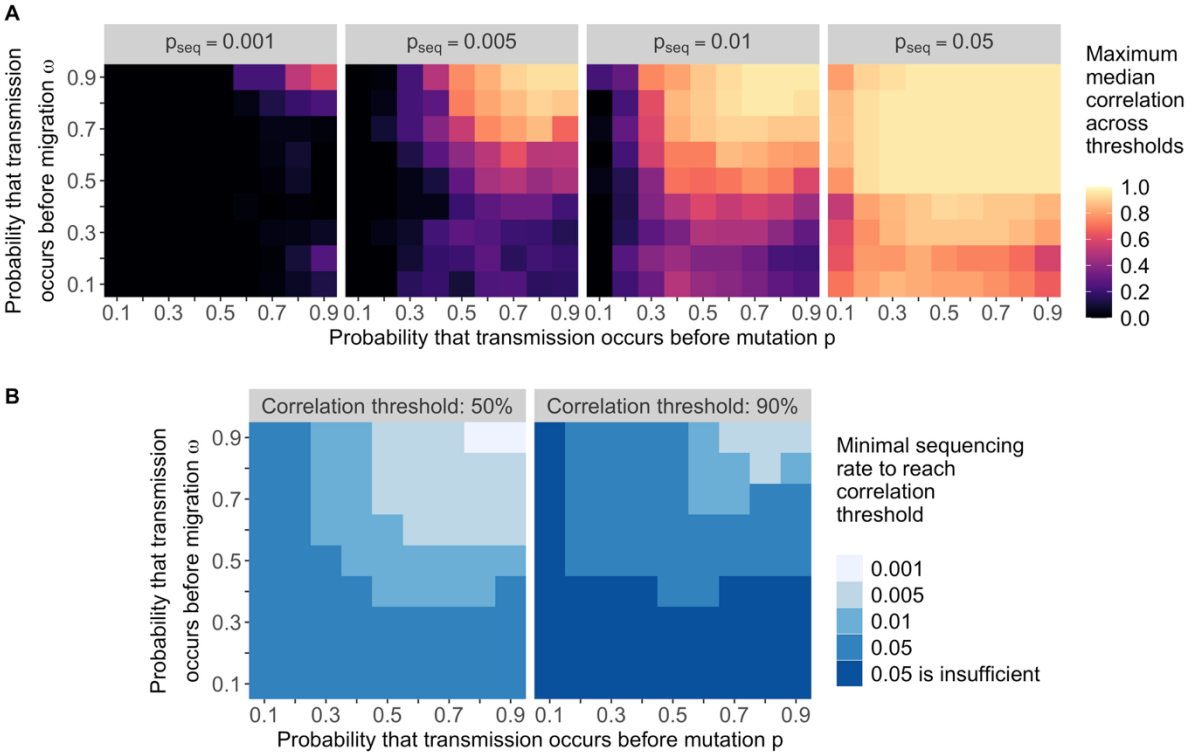

Figure 7: Minimal sampling effort necessary to reach a given phylogeographic inference accuracy. A. Maximum median correlation between the the RR of observing sequences less than Δ mutations away and migration probabilities as a function of of p and ω, across different sequencing fractions p_{seq}. This maximum correlation is computed across genetic distance thresholds Δ ranging between 0 and 15. **B.** Minimal sequencing fraction p_{seq} required to reach a maximum median correlation of 50% or 90%, as a function of of p and ω.

Discussion

In this work, we explore how the complex interplay between transmission, population mixing, mutation and sampling impacts the informativeness of pathogen sequence datasets for understanding population-level epidemic processes. First, we introduce a conceptual framework that uses a confusion matrix approach to quantify whether pairs of sequences are consistent or inconsistent with the underlying migration history. This simple description does not capture richer information contained by genomic data (such as derived sequences or tree branching patterns) but provides a succinct formulation enabling us to comprehensively explore the space of possible phylogeographic analyses by explicitly incorporating the speed at which mutations accumulate within pathogens genome (measured by the probability p that transmission occurs before mutation) and the speed at which pathogens move between population groups (measured by the probability ω that transmission occurs within the same group). Our analyses reveal an inherent limit to the resolution genomic data can provide, particularly when transmission events between population groups occur faster than the accumulation of mutations within pathogen genomes. Second, we complement this theoretical framework with a simulation exercise to investigate how sampling effort and study design impact the accuracy and power of phylogeographic studies based on clusters of genetically proximal sequences. These simulations reveal a second fundamental constraint, with sparser

sampling decreasing the ability of pathogen sequences in deciphering transmission between groups.

Although we focused on approaches that rely on clusters of proximal sequences, the constraints we identified should generalize to methods leveraging genomic data differently. For example, discrete trait analyses (DTAs) rely on richer information encoded in the tree structure but still require branch lengths to be informative about the mixing process. Sequences from a very densely sampled setting where the outbreak is sampled every mutation would thus enable us to characterize mixing processes occurring roughly at the same pace at which mutations accumulate but not faster ones, consistent with the patterns we identified in Figure 4. Furthermore, while we expect sample size requirements to vary between DTAs and methods based on clusters of proximal sequences, sampling can still impact the performance of DTA by increasing branch lengths. Taking the example of a pathogen that would require being sampled every mutation for DTA to shed light on a transmission process of interest, if sampling resulted in branch lengths lying well above this threshold, the final dataset would be insufficient to characterize transmission. Further work directly quantifying such trade-offs for other phylogeographic approaches would be particularly interesting. Overall, while more sophisticated ways of leveraging genomic data may refine inference about transmission processes, some inherent limitations will persist. Awareness of such constraints during study design and analysis is critical to avoid false confidence in the resulting inferences.

While future work should aim at providing robust guidance on power and sample size requirements to characterize population transmission processes, our conceptual framework identifies actionable levers for modulating the power of phylogeographic studies. Sample size and sequencing density in general are major determinants of the power of phylogeographic analyses (Figure 6). However, genomic datasets used to perform such analyses are often repurposed from surveillance efforts or studies not initially aimed at quantifying transmission between groups. Increasing sample size to a desirable level might thus be feasible, particularly for retrospective studies. One alternative is to modify the value of key parameters (assortativity parameter ω and probability that transmission occurs before mutation p) through study design choices. For example, aggregating individuals into broader population groups both increases ω (Figure 4) and decreases the number of between-group mixing rates to estimate. Using WA contact data, we find that analysing age groups in 10-year age bins instead of 5-year ones increases the assortativity parameter ω from 0.35 to 0.48 (Figure 4, Figure S2). Considering spatial spread, we find that aggregating individuals at the PUMA level (around 125,000 inhabitants per PUMA) instead of at the census block group level (around 1,400 inhabitants) increases ω from 0.05 to 0.52 (Figure 4, Table S1). The temporal resolution contained in pathogen sequences is also impacted by the length of the genome analysed, as emphasized by prior work characterizing the value of whole-genome trees relative to gene-specific trees in resolving outbreaks in space and time[6]. In our framework, this would be similar to considering a pathogen characterized by a lower p. For example, influenza A/H3N2 is characterized by a p of 0.82 when concatenating all segments[13] whereas p increases to 0.92 when analysing hemagglutinin segments only. This is congruent with one mutation occurring on average every 19 days across the whole genome versus every 48 days for hemagglutinin segments only.

The inherent limit we identified in analyzing consensus sequences to characterize transmission between population groups underscores the value of developing methods

leveraging identical or nearly identical sequences, particularly in settings characterized by rapid mixing between population groups. Such methods can enable us to get as close as possible to that limit, and prior work has shown promising results to characterize spatial and social mixing from identical SARS-CoV-2 pairs[2]. However, we showed that, even identical sequences may carry insufficient information to reliably estimate population transmission patterns (Figure 4), particularly when mixing occurs rapidly with respect to mutations. Approaches explicitly leveraging within-host diversity and deep-sequencing (thus capturing faster-occurring evolutionary events) could effectively decrease the value of p and have the potential to overcome this limitation.

Overall, our work reveals inherent *horizons of observability* associated with phylogeographic inference that depend on the complex interplay between study design and the relative timescale at which mutation and migration events occur.

Code accessibility: Code to reproduce analyses is publicly available on GitHub at https://github.com/blab/phylogeo-signal.

Author contributions: CTK, JL and TB conceived the study. CTK and JL developed the methods. CTK conducted the analyses. ACP and CTK analysed WA mobility data. CTK, JL and TB interpreted the results. CTK wrote the first draft. All authors edited and reviewed the initial manuscript.

Funding: TB is a Howard Hughes Medical Institute Investigator. This work is supported by NIH NIGMS R35 GM119774. JL acknowledged funding from the Gates Foundation (INV-044865). JL was supported for this work by cooperative agreement CDC-RFA-FT-23-0069 from the CDC's Center for Forecasting and Outbreak Analytics. ACP is supported by the in-house research division of the Fogarty International Center, US National Institutes of Health. CTK and JL would like to thank the Isaac Newton Institute for Mathematical Sciences, Cambridge, for support and hospitality during the programme Modelling and inference for pandemic preparedness, where the work on this paper was initiated. This work was supported by EPSRC grant EP/Z000580/1.

Competing interests: We declare no competing interests.

Disclaimer: The findings and conclusions in this report are solely the responsibility of the authors and do not necessarily represent the official position of the US National Institutes of Health, the Centers for Disease Control and Prevention or the US government.

References

1. Bedford, T. *et al.* Global circulation patterns of seasonal influenza viruses vary with antigenic drift. *Nature* **523**, 217–220 (2015).
2. Tran-Kiem, C. *et al.* Fine-scale patterns of SARS-CoV-2 spread from identical pathogen sequences. *Nature* (2025) doi:10.1038/s41586-025-08637-4.
3. Grubaugh, N. D. *et al.* Tracking virus outbreaks in the twenty-first century. *Nat. Microbiol.* **4**, 10–19 (2019).

4. Grenfell, B. T. *et al.* Unifying the epidemiological and evolutionary dynamics of pathogens. *Science* **303**, 327–332 (2004).
5. Campbell, F., Strang, C., Ferguson, N., Cori, A. & Jombart, T. When are pathogen genome sequences informative of transmission events? *PLoS Pathog.* **14**, e1006885 (2018).
6. Dudas, G. & Bedford, T. The ability of single genes vs full genomes to resolve time and space in outbreak analysis. *BMC Evol. Biol.* **19**, 232 (2019).
7. Wohl, S., Giles, J. R. & Lessler, J. Sample size calculation for phylogenetic case linkage. *PLoS Comput. Biol.* **17**, e1009182 (2021).
8. Mistry, D. *et al.* Inferring high-resolution human mixing patterns for disease modeling. *Nat. Commun.* **12**, 323 (2021).
9. Pullano, G., Alvarez-Zuzek, L. G., Colizza, V. & Bansal, S. Characterizing US spatial connectivity and implications for geographical disease dynamics and metapopulation modeling: Longitudinal observational study. *JMIR Public Health Surveill.* **11**, e64914 (2025).
10. Pullano, G. *US-Connectivity-Metapop*. (GitHub, 2025).
11. Reinhart, A. *et al.* An open repository of real-time COVID-19 indicators. *Proc. Natl. Acad. Sci. U. S. A.* **118**, e2111452118 (2021).
12. Perofsky, A. C. *et al.* Impacts of human mobility on the citywide transmission dynamics of 18 respiratory viruses in pre- and post-COVID-19 pandemic years. *Nat. Commun.* **15**, 4164 (2024).
13. Tran-Kiem, C. & Bedford, T. Estimating the reproduction number and transmission heterogeneity from the size distribution of clusters of identical pathogen sequences. *Proc. Natl. Acad. Sci. U. S. A.* **121**, e2305299121 (2024).
14. Vaughan, T. G. ReMASTER: improved phylodynamic simulation for BEAST 2.7. *Bioinformatics* **40**, (2024).
15. Lee, E., Wohl, S., Giles, J. & McGowan, L. D. *HopkinsIDD/Phylosamp: Phylosamp v1.0.1 (CRAN Release)*. (Zenodo, 2023). doi:10.5281/ZENODO.7964186.

Supplementary information

Supplementary methods

All notations are defined in the main text. To facilitate navigation, a summary of these notations is available in the following table

Parameter	Description
Random variables	
J	Number of jumps separating two infections
M	Number of mutations separating two infections
G	Number of generations separating two infections
Parametrization of the random variables' distribution	
π_g	Probability for two individuals of being separated by g generations
λ	Migration rate
μ	Mutation rate
α	Shape parameter for the Gamma distributed generation time
β	Scale parameter for the Gamma distributed generation time
p	Probability that a transmission event occurs before a mutation one.
ω	Probability that a migration event occurs before a mutation one (assortativity parameter)
Parameters associated with the confusion matrix	
Δ	Genetic distance threshold used to define the linkage criterion
η_Δ	Sensitivity of a linkage criterion defined by a Δ threshold
χ_Δ	Specificity of a linkage criterion defined by a Δ threshold
ϕ_Δ	Positive predictive value of a linkage criterion defined by a Δ threshold

Probabilistic framework detailed derivation

Distribution of the number of jumps conditional on the number of generations.

This is similar to the derivations made in Tran-Kiem et al[2] to calculate the distribution of the number of mutations conditional on the number of generations. Let T^{evo} denote the evolutionary time separating the two individuals we are considering. As the number of jumps follows a Poisson process of rate λ, we have:

$$J \sim \mathcal{P}(\lambda T^{evo})$$

Assuming independence of successive transmission events and because we assumed that the generation time follows a Gamma distribution of parameter (α, β), the time between g successive generations follows a Gamma distribution of shape αg and scale β. Let $f_{x,y}(\cdot)$ denote the probability density function of a Gamma distribution of shape x and scale y. We can derive the distribution of the number of jumps conditional on the number of generations as:

$$P[J = j \mid G = g] = \int_{t=0}^{\infty} P[[J = j \mid G = g, T^{evo} = t] \cdot p(t \mid G = g)\, dt$$
$$= \int_{t=0}^{\infty} \frac{(\lambda t)^j \cdot e^{\lambda t}}{j!} \cdot f_{\alpha g,\beta}(t) dt$$

$$= \int_{t=0}^{\infty} \frac{(\lambda t)^j \cdot e^{\lambda t}}{j!} \cdot \frac{\beta^{\alpha g} \cdot t^{\alpha g - 1} \cdot e^{-\beta t}}{\Gamma(\alpha g)} dt$$
$$= \frac{\lambda^j \beta^{\alpha g}}{j!\,\Gamma(\alpha g)} \int_{t=0}^{\infty} \frac{\Gamma(j+\alpha g)}{(\lambda+\beta)^{j+\alpha g}} \cdot f_{j+\alpha g, \lambda+\beta}(t)\, dt$$
$$= \frac{\Gamma(j+\alpha g)}{j!\,\Gamma(\alpha g)} \cdot \left(\frac{\beta}{\beta+\lambda}\right)^{\alpha g} \cdot \left(\frac{\lambda}{\beta+\lambda}\right)^{j}$$

which is the probability mass function of a negative binomial distribution of parameters $r_{J|g} = \alpha g$ and $p_{J|g} = \frac{\beta}{\beta+\lambda}$.

Therefore:

$$J_{|G=g} \sim NB\left(\alpha g, \frac{\beta}{\beta+\lambda}\right)$$

Distribution of the number of mutations conditional on the number of generations.

By adapting the above demonstration to M, that follows a Poisson process of rate μ, we have:

$$M_{|G=g} \sim NB\left(\alpha g, \frac{\beta}{\beta+\mu}\right)$$

Distribution of the number of jumps conditional on the number of mutations

We introduce $h(k; r, p)$ as the probability mass function, evaluated in k of a negative binomial distribution of parameters r and p. Then, we have:

$$P[J = j \mid M = m] = \sum_{g \geq 1} P[J = j \mid G = g, M = m] \cdot P[G = g \mid M = m]$$
$$= \sum_{g \geq 1} [J = j \mid G = g] \cdot P[M = m \mid G = g] \cdot \frac{P[G = g]}{P[M = m]}$$
$$= \frac{\sum_{g \geq 1} P[J = j \mid G = g] \cdot P[M = m \mid G = g] \cdot P[G = g]}{\sum_{g \geq 1} P[M = m \mid G = g] \cdot P[G = g]}$$
$$= \frac{\sum_{g \geq 1} h\left(j; \alpha g, \frac{\beta}{\beta+\lambda}\right) \cdot h\left(m; \alpha g, \frac{\beta}{\beta+\mu}\right) \cdot \pi_g}{\sum_{g \geq 1} h\left(m; \alpha g, \frac{\beta}{\beta+\mu}\right) \cdot \pi_g}$$

Confusion matrix parameters derivation

Sensitivity

For $\Delta \geq 1$, we have:

$$\eta_\Delta = P[M \leq \Delta \mid J \geq 1]$$
$$= P[M \geq \Delta - 1 \mid J \geq 1] + P[M = \Delta \mid J \geq 1]$$
$$= \eta_{\Delta-1} + \frac{P[J \geq 1 \mid M = \Delta] \cdot P[M = \Delta]}{P[J \geq 1]}$$

We introduce $\eta_\Delta{}'$ as:

$$\eta'_\Delta = \frac{(P[J = 0 \mid M = \Delta] + P[J = 1 \mid M = \Delta]) \cdot P[M = \Delta]}{P[J \geq 1]}$$

Therefore:

$$\eta_\Delta = \eta_{\Delta-1} + \eta'_\Delta$$

We note that $\eta_0 = \eta'_0$. Therefore, for all $\Delta \geq 0$, we have:

$$\eta_\Delta = \sum_{d=0}^{\Delta} \eta_d{}'$$

Specificity

For $\Delta \geq 1$, we have:

$$\begin{aligned}
\chi_\Delta &= P[\,M > \Delta \mid J > 1\,] \\
&= P[\,M > \Delta - 1 \mid J > 1\,] - P[\,M = \Delta \mid J > 1\,] \\
&= \chi_{\Delta-1} - \frac{P[\,J > 1 \mid M = \Delta\,] \cdot P[M = \Delta]}{P[J > 1]} \\
&= \chi_{\Delta-1} - \frac{(1 - P[J = 0 \mid M = \Delta] - P[J = 1 \mid M = \Delta]) \cdot P[M = \Delta]}{1 - P[J = 0] - P[J = 1]}
\end{aligned}$$

For $\Delta \geq 0$, we introduce:

$$\chi'_\Delta = \frac{(1 - P[J = 0 \mid M = \Delta] - P[J = 1 \mid M = \Delta]) \cdot P[M = \Delta]}{1 - P[J = 0] - P[J = 1]}$$

Therefore:

$$\chi_\Delta = \chi_{\Delta-1} - \chi'_\Delta$$

We note that $\chi_0 = 1 - \chi_0{}'$. Therefore, for all $\Delta \geq 0$, we have:

$$\chi_\Delta = 1 - \sum_{d=0}^{\Delta} \chi_d{}'$$

Supplementary tables

Table S1: Estimates of the probability for a movement of occurring within the same geographical unit in the US.

Geographical unit	Data source	Proportion
Census block groups	SafeGraph in Washington state	0.05
Census tracts	SafeGraph in Washington state	0.10
Public Use Microdata Areas (PUMAs)	SafeGraph in Washington state	0.52
Counties	SafeGraph in Washington state	0.81
Counties	Safegraph data from Pullano et al.	0.76
States	Safegraph data from Pullano et al.	0.90

Table S2: Mixing matrix used in the ReMASTER simulations as a function of the assortativity parameter ω used in the parametrization. Each coefficient corresponds to the probability that an infection coming from someone belonging to group i (rows) is in someone in group j (columns).

ω	$(1-\omega)\cdot 1/12$	$(1-\omega)\cdot 4/12$	$(1-\omega)\cdot 7/12$
$(1-\omega)\cdot 1/12$	ω	$(1-\omega)\cdot 7/12$	$(1-\omega)\cdot 4/12$
$(1-\omega)\cdot 4/12$	$(1-\omega)\cdot 7/12$	ω	$(1-\omega)\cdot 1/12$
$(1-\omega)\cdot 7/12$	$(1-\omega)\cdot 4/12$	$(1-\omega)\cdot 1/12$	ω

Supplementary figures

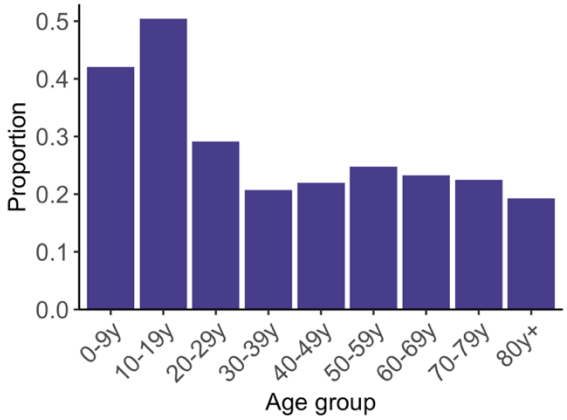

Figure S1: Proportion of contacts occurring within the same age group across age groups, where age group are defined in decades. Estimates were obtained using synthetic social contact data from Washington state[8].

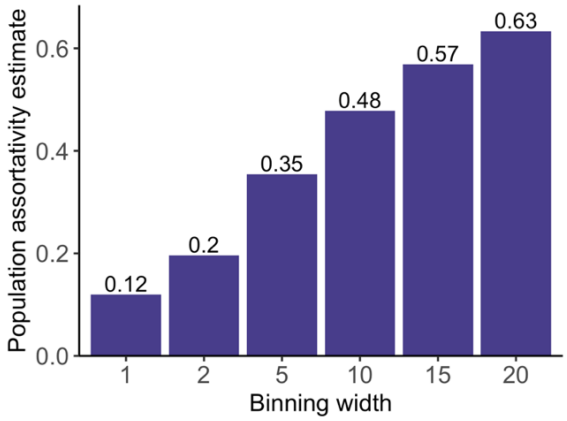

Figure S2: Estimates of the probability for a contact of occurring within the same age group as a function of the binning window width used to define age groups. Estimates were obtained using synthetic social contact data from Washington state[8].

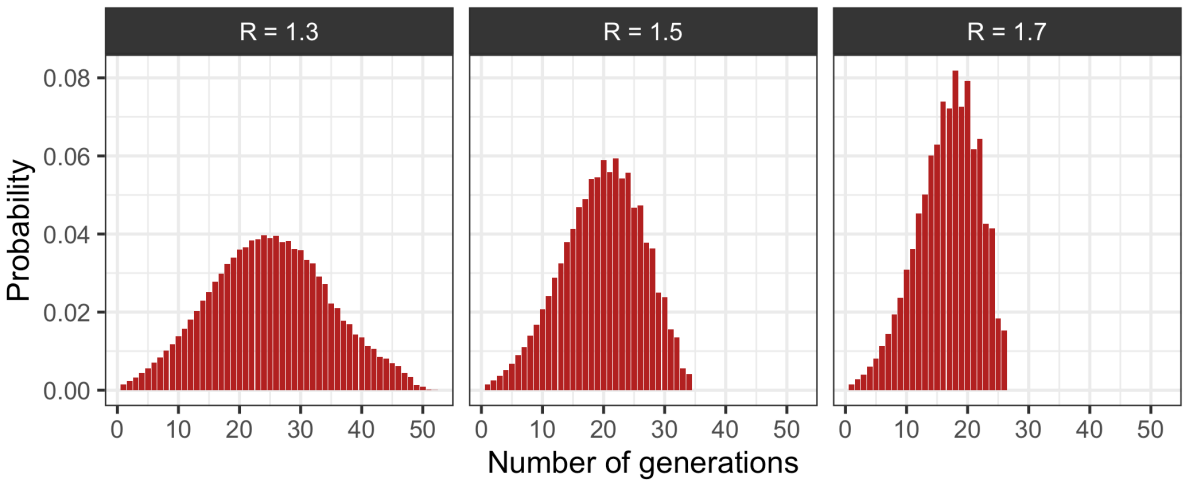

Figure S3: Distribution of the number of generations separating two infected individuals used in the computations. These probabilities are directly extracted from the *phylosamp* R package[15] as estimated by Wohl et al[7].

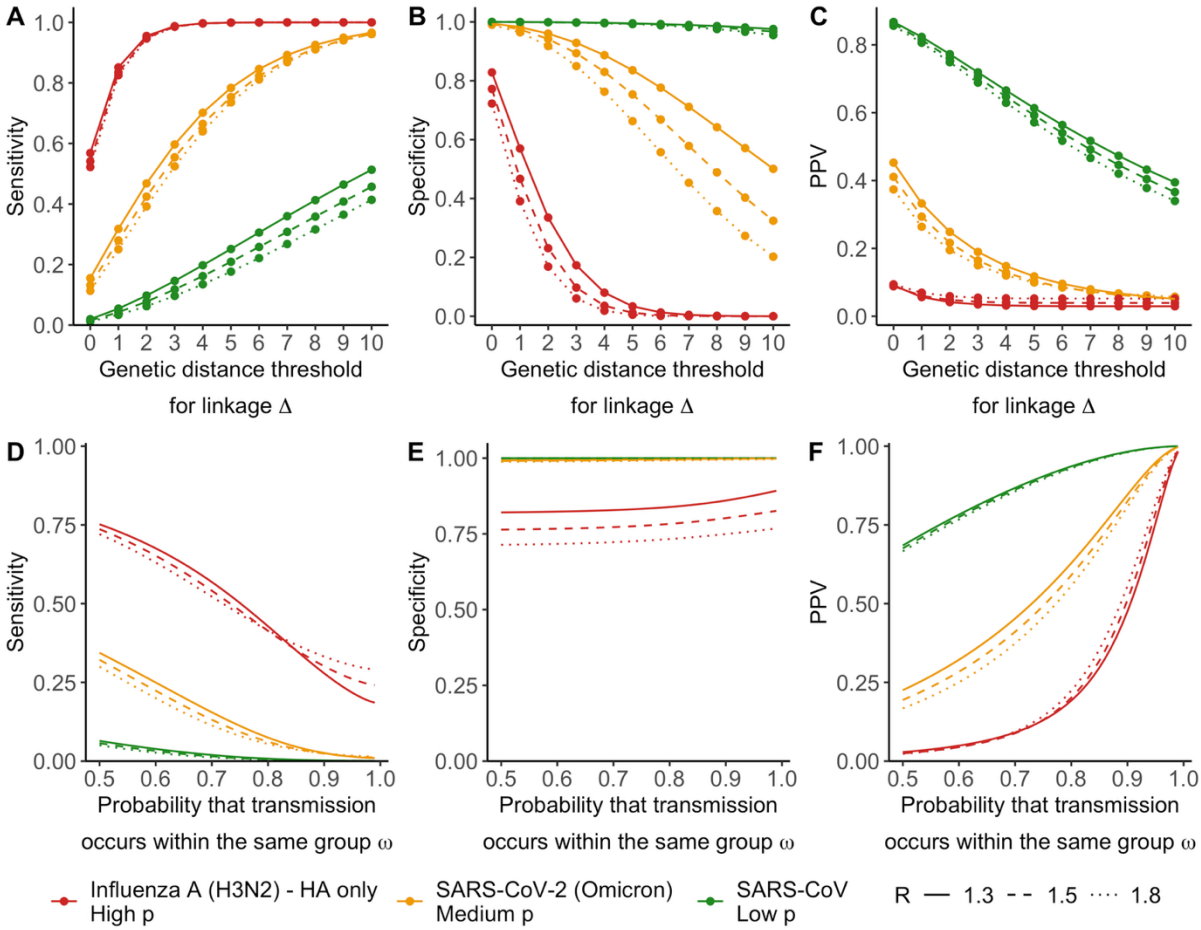

Figure S4: Sensitivity analysis exploring sensitivity, specificity and PPV for different values for the reproduction number R. A. Sensitivity, **B.** specificity and **C.** PPV as a function of the genetic distance threshold used to define the linkage criterion and assuming an assortativity parameter ω of 0.7. **D.** Sensitivity, **E.** specificity and **F.** PPV of a linkage criterion defined by $\Delta = 0$ as a function of the assortativity parameter ω.

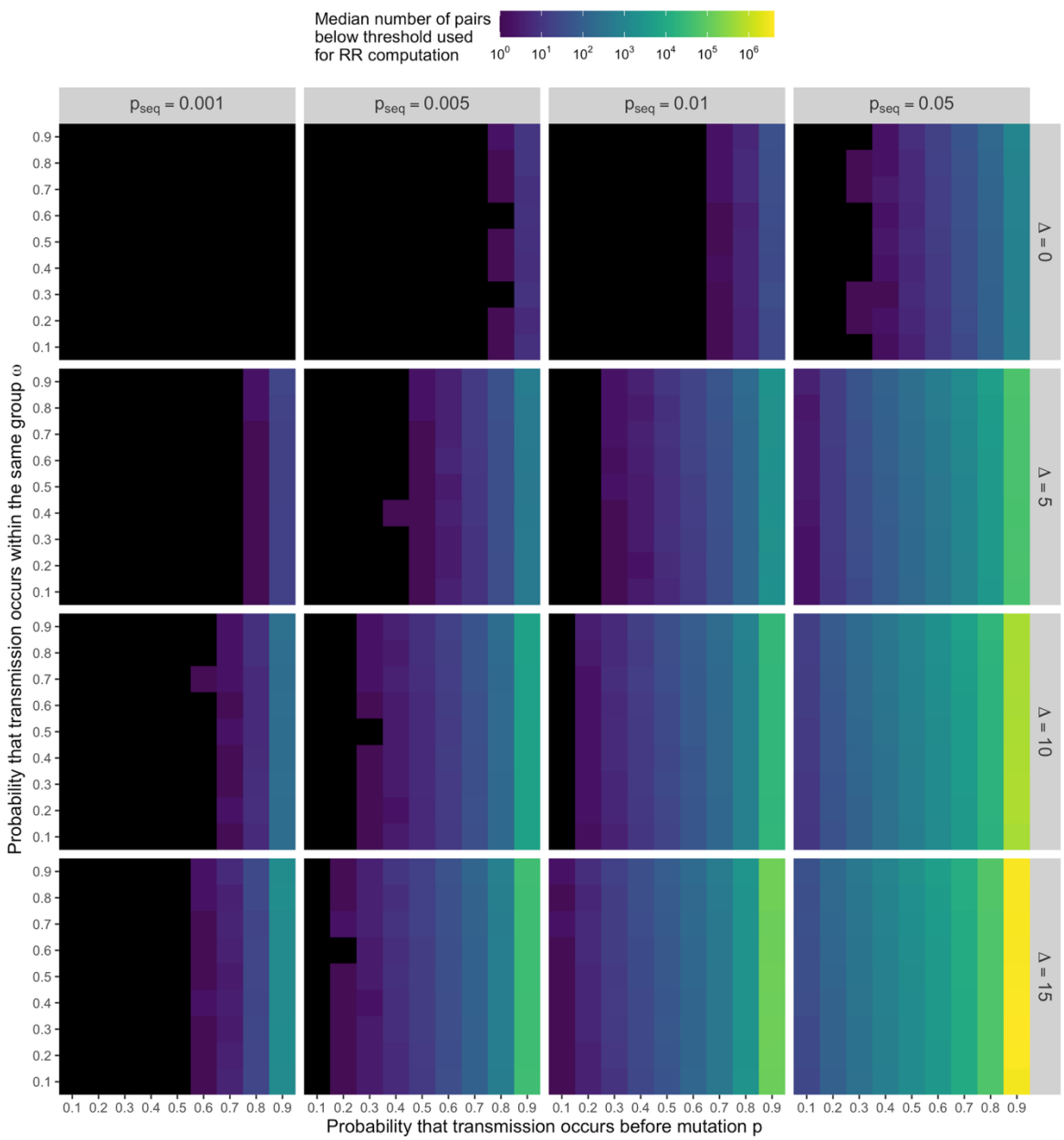

Figure S5: Median number of pairs of sequences less than Δ mutations away across 50 replicate simulations as a function exploring different sequencing fractions p_{seq} and genetic distance thresholds Δ. Results are displayed as a function of p and ω. Black tiles correspond to a median value of 0.